Metallophysics and Advanced Technologies
Металофіз. новітні технол.
Metallofiz. Noveishie Tekhnol.
2025, vol. 47, No. 5, pp. 503–521
https://doi.org/10.15407/mfint.47.05.0503
Reprints available directly from the publisher

PACS numbers: 06.60.Vz, 07.05.Mh, 61.46.-w, 62.23.-c, 65.80.-g, 68.35.Gy, 81.40.Jj

Exploring the Impact of Process Parameters on Tensile Strength in Fused Deposition Modelling: A Comprehensive Study with Predictive Models

K. Zouaoui, S. Amroune, M.-S. Chebbah*, M. Salamani, M. Fnides**, and A. Khaldoune

Laboratory of Materials and Mechanics of Structures, Faculty of Technology, University of M'sila, 28000 M'sila, Algeria.
**Department of Mechanical Engineering, Faculty of Technology, Mohamed Khider University of Biskra, BP 145RP, 07000 Biskra, Algeria*
***Mechanics and Structures Research Laboratory, May 8th 1945 University, 24000 Guelma, Algeria*

Fused deposition modelling or 3*D* printing is a frequently utilized additive manufacturing technique. This approach allows for the creation of lightweight products using various infill strategies and percentages. By adjusting parameters such as temperature, density, speed of printing, *etc.*, components with diverse characteristics can be produced. Polylactic acid (PLA) is favoured for 3*D* printing due to its low cost and sustainability, being derived from renewable sources and biodegradable. Understanding the mechanical performance of different 3*D*-printing strategies is essential for optimizing PLA part production. This study is focused on the application of fused deposition modelling for rapid prototyping and manufacturing, particularly, focusing on the influence of extruder temperature, filling density, and weight on the tensile strength of printed PLA samples. The study is adhered to

Corresponding author: Salah Amroune
E-mail: salah.amroune@univ-msila.dz

Citation: K. Zouaoui, S. Amroune, M.-S. Chebbah, M. Salamani, M. Fnides, and A. Khaldoune, Exploring the Impact of Process Parameters on Tensile Strength in Fused Deposition Modelling: A Comprehensive Study with Predictive Models, *Metallofiz. Noveishie Tekhnol.*, **47**, No. 5: 503–521 (2025). DOI: 10.15407/mfint.47.05.0503

ASTM D-638 tensile standards, with 27 samples printed and tested using an Anycubic i3 Mega machine. The results reveal that extruder temperature minimally affects tensile strength, while filling density has a significant impact, and weight shows no notable effect. Additionally, two predictive models (artificial neural network (ANN) and Taguchi L9) are developed, showing favourable alignment with experimental data, with correlation coefficients reaching 91.03% for the ANN method and 80.75% for stress, 90.13% for strain, and 50.83% for Young's modulus within the Taguchi method.

Key words: fused deposition modelling, mechanical properties, PLA, ANN, Taguchi's method, 3*D* printing.

Моделювання натоплювання або 3*D*-друк є широко використовуваною технікою адитивного виробництва. Цей підхід дає змогу створювати легкі продукти з використанням різних способів заповнення та процентного співвідношення компонентів. Реґулюванням таких параметрів, як температура, густина, швидкість друку та ін., можна виготовляти компоненти з різними характеристиками. Полімолочна кислота (PLA) широко використовується для 3*D*-друку завдяки її низькій вартості та екологічності, оскільки вона одержується з поновлюваних джерел і піддається біологічному розкладанню. Визначення механічних характеристик за різних способів 3*D*-друку має важливе значення для оптимізації виробництва деталів з PLA. Дану роботу спрямовано на використання моделювання натоплювання для швидкого прототипування та виробництва, особливо зосереджуючись на впливі температури екструдера, густині наповнення та ваги на межу міцности друкованих зразків PLA. Під час досліджень було використано стандарти міцности на розтяг ASTM D-638; при цьому 27 зразків було надруковано та протестовано за допомогою машини Anycubic i3 Mega. Результати показують, що температура екструдера та вага мінімально вплинули на межу міцности, тоді як густина наповнення мала значний вплив. Крім того, розроблено два прогностичні моделі (штучна нейронна мережа та Тагучі L9), які демонструють сприятливе узгодження з експериментальними даними з коефіцієнтами кореляції, які сягають 91,03% для методу штучної нейронної мережі та 80,75% для напруги, 90,13% для деформації та 50,83% для модуля Юнґа за моделем Тагучі.

Ключові слова: моделювання натоплювання, механічні властивості, полімолочна кислота, штучна нейронна мережа, метод Тагучі, 3*D*-друк.

(Received 18 May, 2024; in final version, 9 July, 2024)

1. INTRODUCTION

In recent years, there has been a revolutionary shift in the methodologies employed for designing, prototyping, and manufacturing components. Among these techniques, 3*D* printing alternatively referred to as additive manufacturing, stands out as a pivotal technology. Researchers have directed their attention toward investigating this inno-

vative approach due to its capability to craft intricate and sophisticated shapes with a remarkable level of precision [1–3]. This unique and groundbreaking technology transforms conventional manufacturing by constructing objects based on digital models, eliminating the necessity for traditional cutting or casting machines and numerous advantages exist compared to traditional manufacturing methods [4, 5]. The evolution of 3*D* printing encompasses various additive manufacturing (AM) methods, notably fused deposition modelling (FDM), a widely embraced 3*D* printing technique. FDM operates by layering thermoplastic filaments through a computer-controlled extruder nozzle, offering unparalleled flexibility, cost-effectiveness, and user-friendly functionality [6, 7]. Serving as a predominant force in shaping components with intricate designs and integrating diverse materials, it has brought about a revolutionary impact across industries, including biomedical, aerospace, automotive engineering, civil engineering, and beyond [8–10].

Dina *et al.* [11] conducted an investigation to evaluate the effect of different printing parameters on the tensile strength of polylactic acid (PLA) samples manufactured through FDM 3*D* printing. Using a Taguchi array design perpendicular to L25, they systematically examined parameters such as layer thickness, print speed, nozzle temperature, direction angle, and number of lines. The results highlighted the significant influence of printing process variables on tensile strength, revealing values ranging from 37 MPa to 53 MPa. The ideal variables that help achieve maximum tensile strength were also identified, including a layer thickness of 0.22 mm and a printing speed of 45 mm/s, nozzle temperature 205°C, direction angle 70°, use 4 profiles. The tensile test results were compared with predictions generated by both the artificial neural network (ANN) and the mathematical model to validate the results. The maximum error recorded by the artificial neural network was 8.91%, while the maximum error shown by the mathematical model was 19.96%.

Meiabadi *et al.* [12] conducted a study examining the influence of printing angles and UV curing on the mechanical characteristics of FDM fabricated PLA samples. Their investigation focused on assessing the tensile properties of specimens printed at varying angles along *X*-, *Y*-, and *Z*-axes. Noteworthy outcomes from the study indicated a significant impact of printing angles on the tensile behaviour of PLA, particularly, with the *X* 60° specimen demonstrating the highest tensile strength. Additionally, the research revealed that lower infill density and the UV curing process resulted in diminished mechanical properties and material embrittlement, impacting both elongation and Young's modulus.

Another study about the comprehensive examination and design optimization of 3*D* printing structures by scrutinizing the ultimate ten-

sile strength (UTS) of FDM PLA materials across varying printing angles by Tianyun *et al.* [13]. Notably, the findings revealed a significant alteration in the UTS of 3*D*-printing materials corresponding to changes in the printing angle. The study observed a consistent decrease in tensile strength as the layer thickness increased from 0.1 mm to 0.3 mm. Particularly, noteworthy is the substantial UTS gap of 52.29%, observed between 0° and 90° 3*D*-printing materials with a layer thickness of 0.1 mm.

Muammel *et al.* [14] investigated a study to explore the influence of diverse 3*D*-printing process parameters on the tensile strength and hardness properties of PLA, employing FDM technique. Their investigation encompassed the examination of various build orientations, raster direction angles, and layer heights. The results obtained from the study revealed that the on-edge orientation samples exhibited the highest values for Young's modulus and ultimate tensile strength, measuring at 1.896 ± 0.044 GPa and 49.12 ± 0.78 MPa, respectively. Furthermore, the specimen with a 0.1 mm layer thickness demonstrated the most favourable elongation at break, reaching 3.13%.

The examination of existing literature indicates a limited number of research studies addressing advancements in additive manufacturing specifically using fused deposition modelling (refer to Fig. 1). Therefore, the present study strategically directs its attention towards investigating the influence of extruder density, printing temperature, and weight on the tensile strength of PLA samples.

The uniqueness of this study lies in its thorough examination of the application of FDM for rapid prototyping and manufacturing, with a particular emphasis on three key parameters: extruder temperature, filling density, and weight. While most previous studies typically focus on one or two of these parameters, this research deliberately ex-

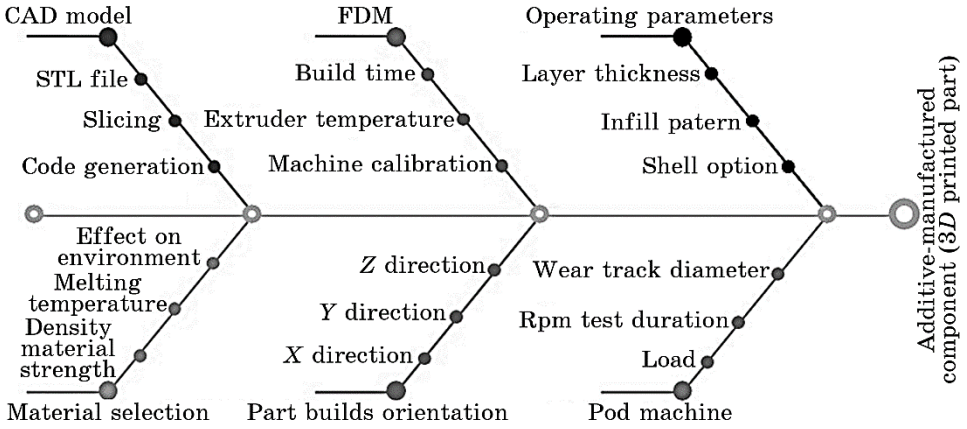

Fig. 1. Cause and effect diagram of FDM process parameters.

plored the interaction among these variables and their impact on the tensile strength of printed PLA samples. Furthermore, the use of ASTM D-638 tensile standards ensures compliance with recognized testing protocols, thereby reinforcing the reliability of the results. The implementation of two predictive models, namely ANN and Taguchi, to interpret experimental data strengthens the robustness of the analysis.

2. MATERIALS AND METHODS

2.1. Samples Preparation

In this work, we drew all the samples in CATIA CAD software. After that we converted the CAD file to STL format, and we configured the printing settings through Ultimaker Cura and using the Anycubic i3 Mega printer according to ASTM D638 Type IV (this test method for analysing tensile property data for plastic materials) [15] (Fig. 2). Using PLA filament to determine the printing temperature and PLA filament density impact on tensile strength.

The Anycubic i3 Mega is a Cartesian-style FDM printer that utilizes a heated bed and a single extruder to deposit thermoplastic materials, allowing the creation of 3*D* objects [16]. Impression size is not more than 210×210×205 mm^3, 1.75 mm diameter filament suitable for PLA, ABS, HIPS, PETG, and wood, with 0.4 mm buse that can reach 260°C. The heating plate reaches 110°C and prints the objects from an SD card or USB cable.

PLA filament is a frequently used 3*D* printing material. PLA is a thermoplastic produced using renewable resources like cornstarch, sugar cane, tapioca roots, and potato starch, and the technical properties of PLA filament in Table 1 [17].

The infill pattern (zigzag) and bed temperature is of 60°C. The layer thickness and orientation angle were constants (Table 1). The samples were printed according to three temperatures (200°C, 210°C, 220°C) and three densities (20%,30% and 40%), which means 27 specimens

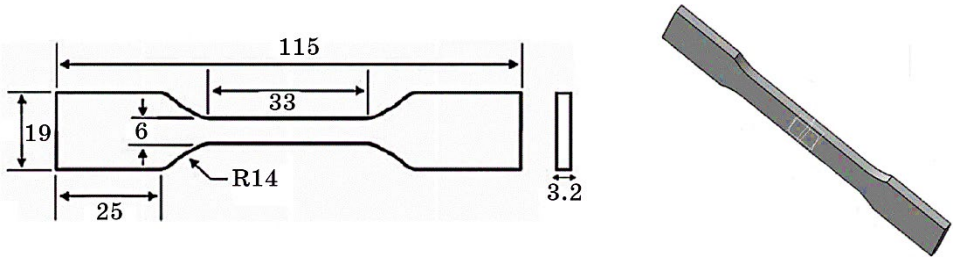

Fig. 2. CAD model and specification of tensile specimen.

TABLE 1. PLA technical properties and fixed printer settings.

Filament specifications	Values	Settings	Specification
Diameter	1.75 mm	Speed printing, mm/s	70
Length	$330 \cdot 10^6$ µm	Wall thickness, mm	1.2
Weight	1 kg for each spool	Infill pattern	zigzag
Density	1.24 g/cm^3	Build plate temperature, °C	60
Tensile strength	62 kg/cm^2	Fan speed, %	100
Flexural modulus	28000 kg/cm^2	Layer height, mm	0.2
Colour	PLA Green	Initial layer speed, mm/s	10

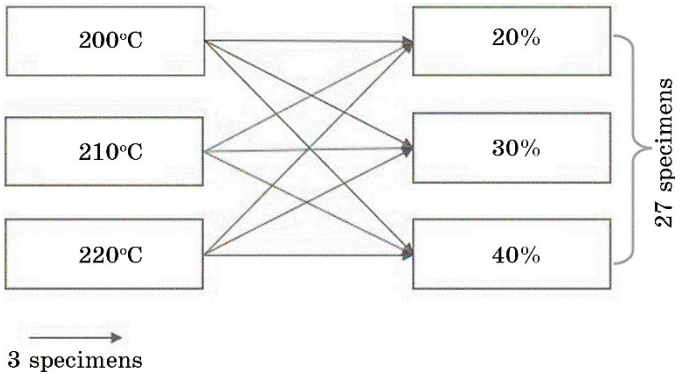

Fig. 3. Printing parameters for samples.

printing as follows (Fig. 3).

2.2. Tensile Test

The 27 printed samples (Fig. 4, *b*) were testing on the universal testing machine (Test 112) with a speed of 0.1 mm and force of 5 kN for tensile strength keeps at the completely tensile course (Fig. 4, *c*, *d*). The inherent software module meticulously logged the data pertaining to the utmost tensile strength, elongation, and force load. The results of tensile strength of the tensile strength are shown in Table 2.

The calculation of stress (σ) during tensile testing is succinctly articulated through the fundamental formula as Eq. (1):

$$\sigma = F/A, \tag{1}$$

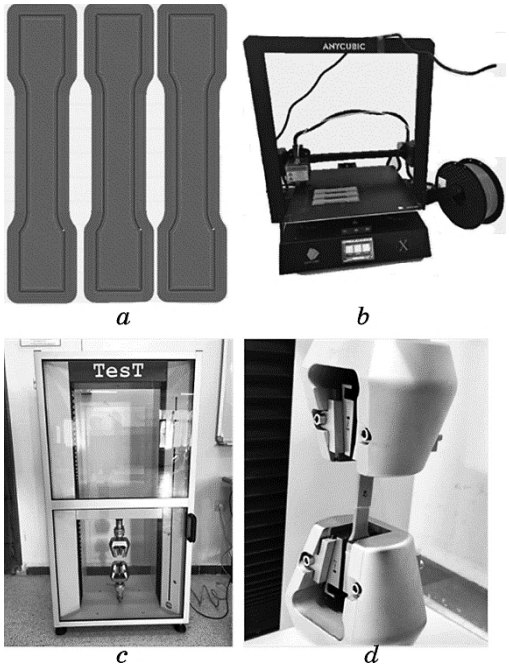

Fig. 4. Tensile test procedure.

signifies the cross-sectional area of the specimen. It is an important mechanical property of materials that is used to describe their resistance to deformation and failure under tensile forces. This formula applies to homogeneous materials with uniform cross-sections and is valid only up to the point of fracture. Beyond the point of fracture, the material undergoes plastic deformation, and the stress-strain relationship becomes nonlinear. The tensile stress formula is widely used in various fields, such as engineering, physics, and materials science, to characterize the mechanical behaviour of materials under tensile forces. It is also used to design and optimize structures and components that are subjected to tensile loads, such as bridges, buildings, and aircraft [18].

2.3. Artificial Neural Network (ANN)

Artificial neural networks (ANNs) serve as a mathematical instrument inspired by the structure and function of the human brain and biological nervous system [19]. They are composed of interconnected nodes, or neurons, that process and transmit information through weighted connections. ANNs are capable of learning from data, recognizing patterns, and making predictions or decisions based on the input–output relationships.

TABLE 2. Empirical and anticipated tensile strength of pla samples using ann model.

No	Temperature (°C)	Density (%)	Weight (g)	Strain (mm)			Stress (MPa)			Young's modulus×10^{-3} (GPa)		
				Exp	ANN	Err	Exp	ANN	Err	Exp	ANN	Err
1	200	20	4.881	0.011	0.012	−0.001	32.29	43.36	−11.07	2630.20	2737.87	−107.67
2	200	20	4.871	0.010	0.012	−0.001	30.46	43.27	−12.81	2774.20	2753.13	021.07
3	200	20	4.895	0.011	0.012	−0.001	32.05	43.49	−11.44	2755.60	2718.32	037.28
4	200	30	5.081	0.009	0.015	−0.006	28.96	43.00	−14.04	2956.90	2575.81	381.09
5	200	30	5.122	0.012	0.015	−0.003	37.07	43.46	−6.39	2696.20	2548.85	147.35
6	200	30	5.105	0.012	0.015	−0.003	34.59	43.29	−8.70	2760.80	2555.83	204.97
7	200	40	5.403	0.014	0.013	0.001	42.13	44.16	−2.04	2747.40	2753.22	−005.82
8	200	40	5.409	0.013	0.013	0.000	39.70	44.21	−4.51	2877.60	2755.92	121.68
9	200	40	5.405	0.016	0.013	0.003	44.74	44.18	0.56	2368.70	2754.12	−385.42
10	210	20	4.887	0.011	0.010	0.001	32.58	32.54	0.04	2756.40	2775.05	−018.65
11	210	20	4.887	0.010	0.010	0.000	29.69	32.54	−2.84	2803.90	2775.05	028.85
12	210	20	4.868	0.011	0.009	0.002	32.78	32.43	0.34	2754.10	2804.92	−050.82
13	210	30	5.145	0.011	0.014	−0.003	35.36	32.79	2.58	2901.80	2768.98	132.82
14	210	30	5.149	0.012	0.014	−0.002	36.16	32.81	3.35	2727.90	2764.46	−036.56
15	210	30	5.131	0.011	0.014	−0.003	34.70	32.69	2.01	2952.70	2785.26	167.44
16	210	40	5.400	0.013	0.010	0.003	40.60	32.16	8.43	2711.80	2669.00	042.80
17	210	40	5.405	0.013	0.010	0.003	41.87	32.24	9.63	2823.40	2662.23	161.17
18	210	40	5.395	0.012	0.010	0.002	38.74	32.09	6.65	2949.70	2676.19	273.51
19	220	20	4.859	0.010	0.009	0.001	30.82	29.61	1.21	2785.10	2786.62	−001.52
20	220	20	4.856	0.011	0.009	0.002	32.25	29.62	2.64	2750.20	2787.19	−036.99
21	220	20	4.851	0.011	0.009	0.001	31.50	29.63	1.87	2764.50	2788.06	−023.56
22	220	30	5.153	0.012	0.010	0.003	37.76	29.19	8.57	2818.50	2745.07	073.43
23	220	30	5.122	0.012	0.010	0.003	37.01	29.24	7.77	2764.20	2761.36	002.84
24	220	30	5.398	0.012	0.009	0.003	36.19	29.01	7.18	2759.60	2746.59	013.01
25	220	40	5.386	0.011	0.009	0.001	34.91	29.10	5.81	3013.20	2964.64	048.56
26	220	40	5.401	0.012	0.009	0.003	37.71	29.09	8.62	2864.60	2956.48	−091.88
27	220	40	5.410	0.012	0.009	0.003	38.51	29.09	9.42	2942.50	2950.75	−008.25

ANNs have been widely used in various fields, such as computer vision, natural language processing, speech recognition, and robotics, to solve complex problems that are difficult or impossible to solve using traditional algorithms [20, 21]. The function ANN method is employed for output prediction. This neural network comprises three layers, namely, an input layer, an output (or target) layer, and an intervening hidden layer. The number of input and output parameters related by the quantity of neurons in the input and output layers.

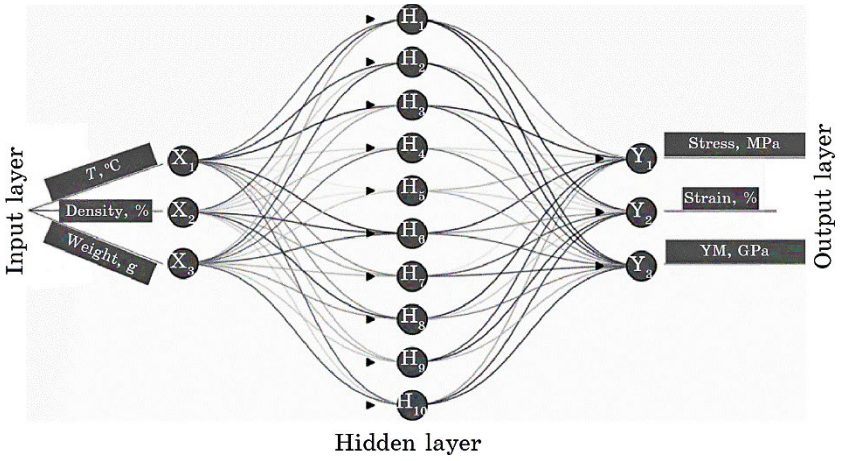

Fig. 5. Schematic of the ANN.

In this study, ANN model underwent training using MATLAB, incorporating input parameters such as temperature, density, and sample weight, along with output parameters including stress modulus, strain, and Young's modulus. The neural synthesis tool facilitated the importation of a 3×27 input matrix and corresponding 3×27 output data, as illustrated in Fig. 5.

2.4. Taguchi Method

The Taguchi method, created by Japanese engineer Genichi Taguchi, is recognized as a robust engineering tool for enhancing the quality of engineering design by integrating statistical methods and concepts from design of experiments. It has demonstrated successful application across various domains such as manufacturing and engineering, product design, experimental design, reliability engineering, and chemical process design, specifically in maximizing yields of specific compounds. The approach advocates notable advancements in three key design phases: system design, parameters design, and tolerance design [22, 23].

In this work, the experiments were arranged using Taguchi's orthogonal array of fractional factorial design (L9) with the assistance of Minitab software.

The Taguchi method entails performing experiments to optimize the printing process by adjusting input factors to attain the targeted S/N ratio. By emphasizing the S/N ratio, the Taguchi method seeks to enhance quality, robustness, and performance while mitigating the impact of variability and external factors. Given that this investigation

focuses on maximizing stress, strain, and Young's modulus values, the data points are computed using a 'bigger is better' approach to attain superior performance and reduced sensitivity to variation. This categorization ensures that the S/N ratio is characterized as Eq. (2):

$$\frac{S}{N} = -10 \log_{10} \left(\frac{1}{n} \sum_{i=1}^{n} \left(\frac{y_i}{\sigma} \right)^2 \right), \tag{2}$$

where y_i represents the mean of measurements for each trial, and σ is the standard deviation [24, 25].

3. RESULTS AND DISCUSSION

3.1. Tensile Strength

Following the execution of a tensile test on the 27 specimens (Fig. 6), the experimental findings depicted in Figs. 7 and 8 were ascertained. Notably, the density exhibited a noteworthy influence on the strain, Stress, and Young's modulus (output parameters), when juxtaposed with the temperature. This observation underscores that an augmentation in the density value corresponds to an escalation in the three output parameters. For instance, at a density of 20% and a temperature of 200°C, the strain, stress, and Young's modulus registered values of 0.010%, 30.46 MPa, and 2774 MPa, respectively. These values exhibited an increase to 0.013%, 39.70 MPa, and 282877 MPa at the same temperature but with a density of 40%.

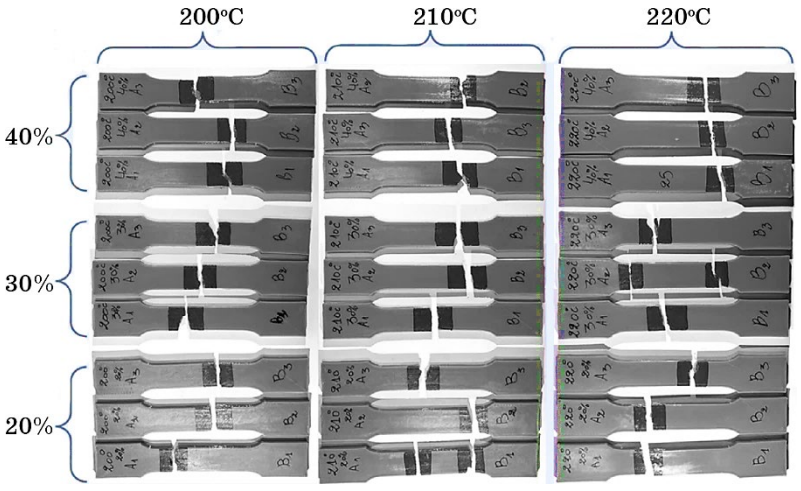

Fig. 6. Samples after testing on tensile test machine.

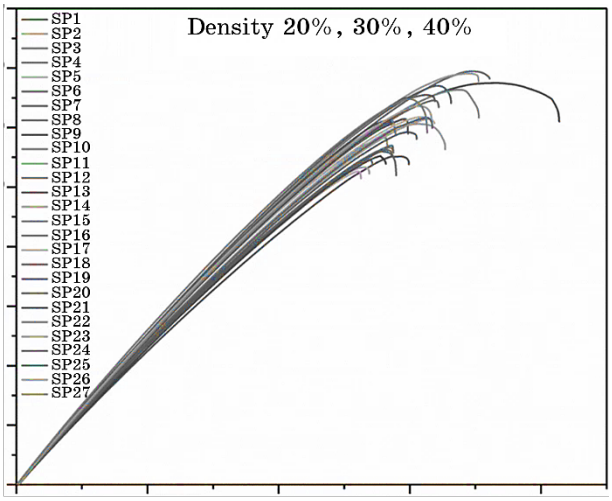

Fig. 7. Stress (MPa)–strain (%) curve for experimental condition (27 specimens).

Conversely, a rise in temperature was correlated with a reduction in strain and stress. Notably, at a temperature of 200°C and a density of 20%, the strain, tensile strength, and Young's modulus were recorded at 0.011%, 32.29 MPa, and 2630.20 MPa, respectively. However, these values experienced a decrease to 0.010% and 30.82 MPa at a temperature of 220°C and a density of 20%, while concurrently, the value of Young's modulus increased to 2785.10 MPa under identical printing conditions.

3.2. ANN Results

Figure 9, *a* illustrates the mean squared error (MSE) values across different epochs (Eq. (3)). A decreased MSE corresponds to an increased accuracy in predictions made by (ANN) model [26, 27]. Notably, during observations, the MSE exhibited significant values, approximately 3.2705 for training, $4.527 \cdot 10^{-1}$ for validation, and 8.1064 for testing. The training and validation processes concluded after 7 iterations, as depicted in Fig. 9, *b*. The optimization was achieved with a validation score of 0.00070939, observed at the eleventh iteration through gradient analysis. This point was deemed optimal by the artificial neural network:

$$MSE = \frac{1}{n}\sum_{i=1}^{n}\left|(y_i - \hat{y}_i)^2\right|, \tag{3}$$

where n is the number of observations in the dataset, y_i is the actual

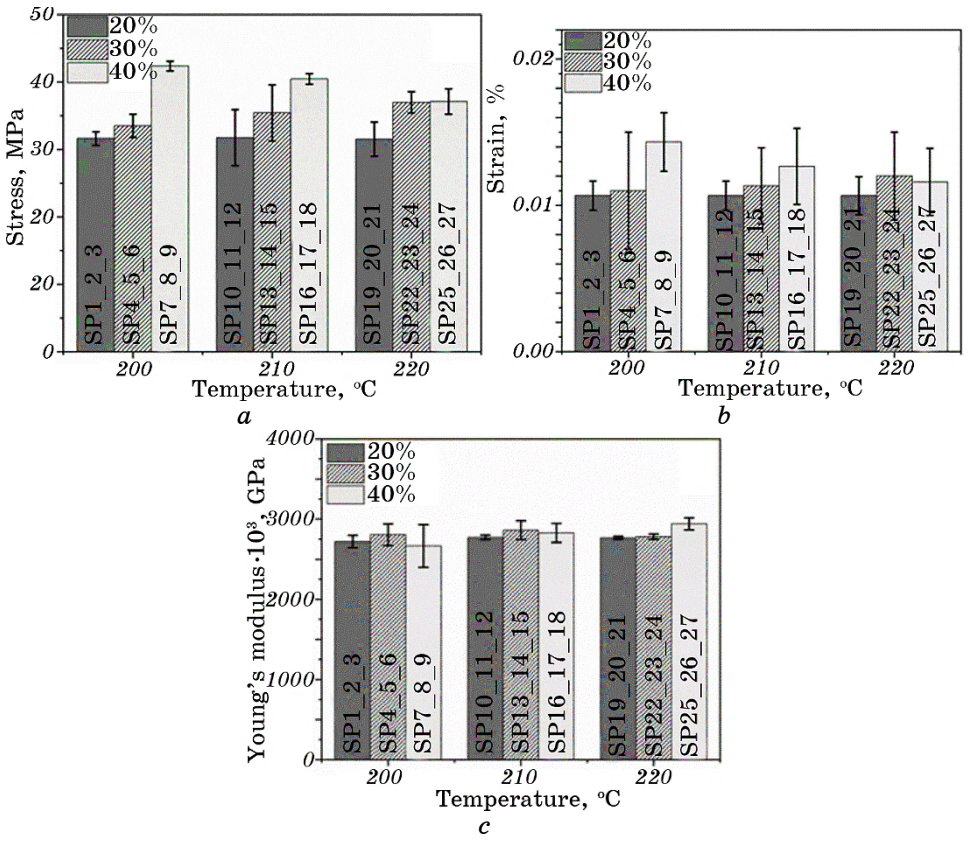

Fig. 8. Stresses (MPa) and strains (%) data for experimental condition (27 specimens).

target value for observation i, and $\hat{y}_i$ is the value predicted by the model for observation i [28].

In contrast, Fig. 10 displays the R coefficient values concerning the target. Achieving minimal error necessitates that the total R value in training, testing, and validation schemes be close to 1 [29]. Remarkably, the ANN model demonstrated a notably high correlation coefficient, reaching 0.960623, 0.94826, and 0.9103 for training, validation, and testing, respectively (Eq. (4)). Table 2 illustrates a comparison between the actual experimental data for the average values of stress, strain, and Young's modulus and the corresponding anticipated values generated by ANN. Evidently, there is a remarkable proximity between the experimental and predicted data, characterized by an exceptionally small error deviation. The average error, quantified at $3 \cdot 10^{-5}$, further emphasizes the close agreement between the observed and forecasted values:

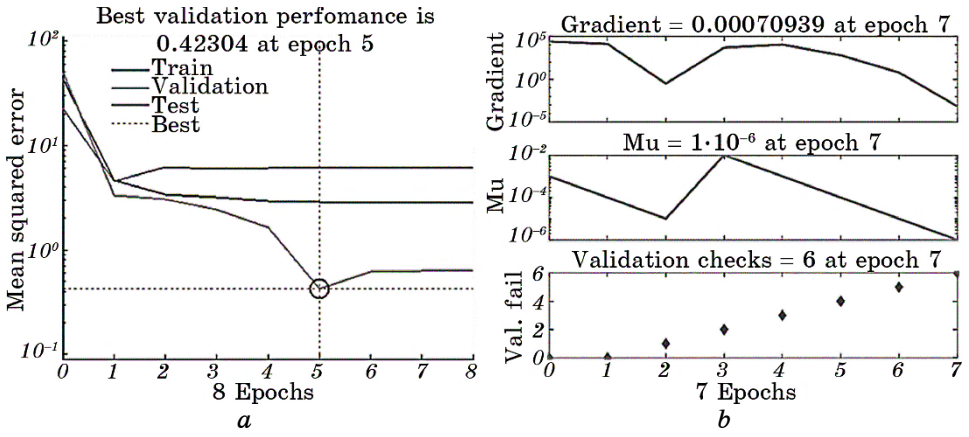

Fig. 9. Cumulative mean squared errors across epochs in network data.

$$R^2 = 1 - \sum_{i=1}^{n} (y_i - \hat{y}_i)^2 \,/\, \sum_{i=1}^{n} (y_i - \bar{y}_i)^2, \tag{4}$$

where n is the number of observations, y_i is the actual target value for observation i, $\hat{y}_i$ is the predicted value by the model for observation i, and $\bar{y}_i$ is the mean of the actual values.

3.3. Taguchi Results

Figures 11, *a–c* depict the outcomes and recommendations derived from the application of the Taguchi method concerning strain, stress, and Young's modulus values as a function of temperature, density, and weight, respectively. The influence of density on various outcomes is noteworthy, with higher density values correlating to increased strain, stress, and Young's modulus. For instance, at 20%, the corresponding values were 0.011% for strain, 31 MPa for stress, and 2750 MPa for Young's modulus, compared to 0.013%, 40 MPa, and 2800 MPa at 40%. Additionally, temperature exhibited a notable impact on these parameters, as elevated temperatures decreased strain and stress, while Young's modulus saw an increase in values. At 200°C, the values were 0.012%, 36 MPa, and 2730 MPa; at 220°C, they were 0.011%, 35 MPa, and 2850 MPa. Conversely, the weight factor displayed irregular behaviour in the three outputs.

Figures 11, *d–f* depict the residual plots for strain, stress, and Young's modulus. By examining the normal probability plot of residuals, it becomes evident that the points closely align with a straight line, affirming the normal distribution of residuals for all output parameters.

Analysing the histogram of residuals provides insight into the da-

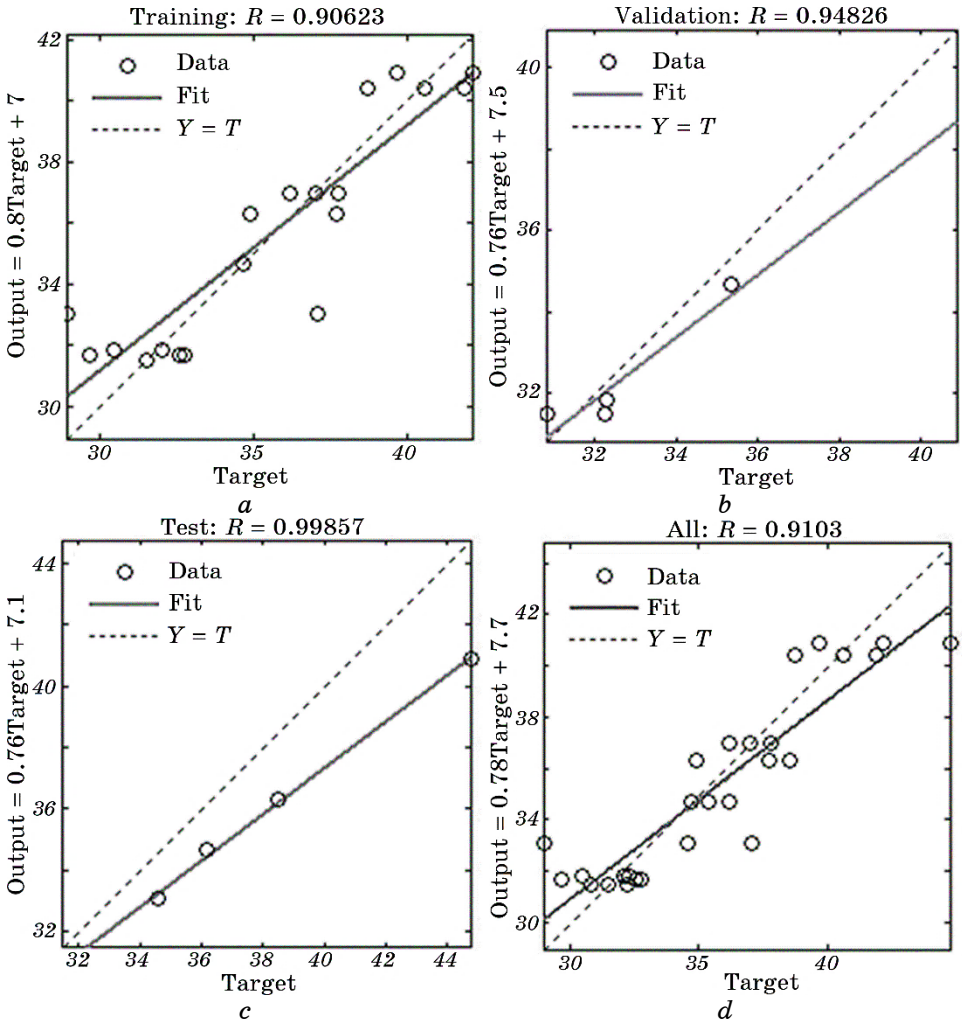

Fig. 10. Neural network regression graph.

ta's general characteristics, encompassing typical values, spread, and shape. Notably, the presence of long tails in the plot suggests significant skewness in the data.

Considering the waste versus order plot, a tool for identifying non-random errors, rapid changes in successive residues' signs reveal a negative correlation in strain and stress. In contrast, Young's modulus exhibits a positive correlation, as the majority of residues share the same sign.

The residuals versus fits plot is expected to display a random pattern of residuals on both sides of zero. However, the observed series of increasing

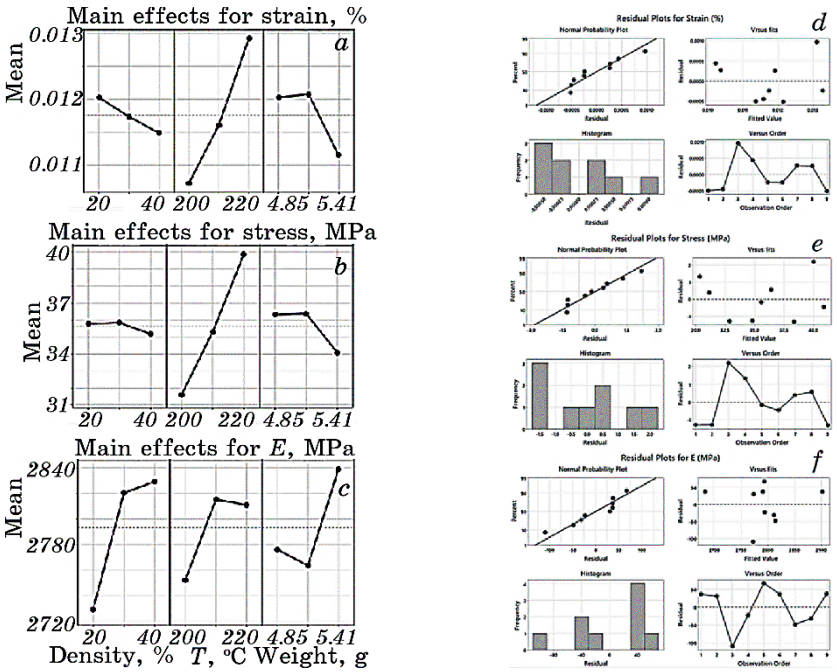

Fig. 11. Plot depicting the primary effects of the input variables and residual plots.

and decreasing points indicates a prevalence of positive residuals over negative ones, pointing towards a non-random nature of the errors.

The optimal parameters were determined by selecting the highest signal-to-noise (S/N) ratio for each factor, chosen to maximize the output parameters, as illustrated in Table 3. The values presented in Table 3 represent average measurements derived from three samples (L9) for each type of PLA sample. The optimal parameters include a maximum strain (ε) of 0.0140 MPa and stress (σ) of 42.1891 MPa achieved in run 3, with corresponding S/N ratios of –37.0284 and 32.5040, respectively. In contrast, a minimum strain of 0.0106 MPa and stress of 31.5246 MPa were attained in run 9, accompanied by S/N ratios of –39.45808 and 29.97301, respectively. The maximum Young's modulus, reaching 2940.1 MPa, was observed in run 3 with an associated S/N ratio of 69.3672, while the minimum Young's modulus of 2664.5666 MPa was recorded in the initial run, correlating with an S/N ratio of 68.5125. The findings demonstrated a robust alignment between the model and experimental data, showcasing correlation coefficients of 80.75% for stress and 90.13% for strain. However, a comparatively lower value of 50.83% was observed for Young's modulus. Table 4 presents the regression equation for strain, stress, and Young's modulus factor as functions of the three preceding factors.

TABLE 3. Tensile test results incorporating the S/N ratio and tensile predicted values of strain, stress and Young's modulus.

No.	T, °C	D, %	W, g	ε (exp.), %	σ (exp.), MPa	E (exp.), MPa	S/N (ε)	S/N (σ)	S/N (E)	ε (pr.), %	σ (pr.), MPa	E (pr.), MPa
1	200	20	4.85	0.0108	31.597	2720.0	–39.2	29.9	68.6	0.0112	32.5110	2672.7
2	210	20	5.41	0.0111	33.540	2804.6	–39.0	30.5	68.9	0.0112	33.9823	2797.8
3	220	20	5.14	0.0140	42.189	2664.5	–37.0	32.5	68.5	0.0135	40.8340	2718.6
4	200	30	5.41	0.0106	31.683	2771.4	–39.4	30.0	68.8	0.0101	30.3284	2825.5
5	210	30	5.14	0.0115	35.409	2860.8	–38.7	30.9	69.1	0.0119	36.3227	2813.5
6	220	30	4.85	0.0130	40.401	2828.3	–37.6	32.1	69.0	0.0131	40.8436	2821.4
7	200	40	5.14	0.0106	31.524	2766.6	–39.4	29.9	68.8	0.0107	31.9664	2759.7
8	210	40	4.85	0.0121	36.984	2780.7	–38.2	31.3	68.8	0.0116	35.6299	2834.8
9	220	40	5.41	0.0116	37.045	2940.1	–38.6	31.3	69.3	0.0120	37.9585	2892.8

The obtained results align with Kafshgar *et al.* findings [30], as determined through ANOVA and the Taguchi method. Consistencies were observed in the behaviour of UTS, modulus of elasticity, and yield strength with variations in process parameters. The peak values were identified at an infill density of 60%, extrusion temperature of 220°C, raster angle of 90°, and layer thickness of 0.1 mm. Similarly, elongation at break and toughness exhibited analogous patterns, reaching their highest levels at an infill density of 60%, extrusion temperature of 200°C, raster angle of 45°, and layer thickness of 0.2 mm.

Nugroho *et al.* [31] determined that tensile strength is primarily influenced by infill density, followed by nozzle temperature, infill pattern, and extrusion width. The optimized parameters yielding a tensile strength of 30.52 MPa at a 95% confidence interval were identified as 75% infill density (C3), 215°C nozzle temperature (A3), honeycomb infill (D1), and 0.3 mm extrusion width (B1). Both printing temperature and density emerged as pivotal factors.

Abdulridha *et al.* [32] reported a tensile strength of 55 MPa in their investigation of PLA parts manufactured by FDM printing. The high-

TABLE 4. The regression equation for strain, stress, and Young's modulus factor as functions of the three input factors.

Taguchi response	Regression equation
Strain	$-0.000027 - 0.00256D + 0.00011T - 0.0015551W$
Stress	$-30.2 - 0.0295D + 0.4138T - 3.95W$
Young's modulus	$1470 + 4.97D + 2.92T + 109W$

est value was achieved with 80% density, a grid-filling pattern, layer thickness of 0.25 mm, shell thickness of 0.8 mm, six upper and lower layers, and a filling overlap of 10%.

Teharia *et al.* [33] focused on optimizing PLA-based tensile specimens using FFF technology. Their results indicated that the ideal process parameters for high tensile strength are layer thickness of 200 μm, nozzle temperature of 210°C, speed/feed rate of 50 mm/min, grid filling pattern, and point direction of 0°. The ANN analysis further contributed to identifying optimal parameters, with R-values of 95%, indicating minimal error.

4. CONCLUSIONS

This study investigates the tensile strength of a PLA specimen produced through an FDM 3D printer, employing both experimental and statistical analyses with a focus on three process parameters. The experiments were designed using Taguchi and ANN methodologies. The ensuing conclusions are as follows.

Density significantly influences strain, stress, and Young's modulus. Higher density values correlate with increased values for these three output parameters. At 20% density and 200°C, the values were 0.010% strain, 30.46 MPa stress, and 2774 MPa Young's modulus. At 40% density and the same temperature, values increased to 0.013% strain, 39.70 MPa stress, and 282877 MPa Young's modulus.

Rise in temperature led to a reduction in strain and stress. At 200°C and 20% density, values were 0.011% strain, 32.29 MPa stress, and 2630.20 MPa Young's modulus. At 220°C and the same density, strain decreased to 0.010%, stress to 30.82 MPa, while Young's modulus increased to 2785.10 MPa.

Optimization was achieved with a validation score of 0.00070939 at the eleventh iteration through gradient analysis, identified as the optimal point by the ANN.

The ANN model demonstrated high correlation coefficients of 0.960623, 0.94826, and 0.9103 for training, validation, and testing, respectively. Remarkably close agreement between experimental and predicted data is evident, characterized by an exceptionally small average error deviation of $3 \cdot 10^{-5}$.

Optimal parameters were determined by selecting the highest signal-to-noise (S/N) ratio for each factor to maximize the output parameters. The highest strain (0.0140 MPa) and stress (42.1891 MPa) were achieved in run 3 with S/N ratios of –37.0284 and 32.5040, respectively. The lowest strain (0.0106 MPa) and stress (31.5246 MPa) were attained in run 9 with S/N ratios of –39.45808 and 29.97301, respectively. Maximum Young's modulus (2940.1 MPa) was observed in run 3 with an S/N ratio of 69.3672, while the minimum (2664.5666 MPa)

was recorded in the initial run with an S/N ratio of 68.5125.

This contribution was created under the support of the PRFU Project A11N01UN280120230002 organized by the Algerian Ministry of Higher Education and Scientific Research.

REFERENCES

1. P. Wu, J. Wang, and X. Wang, *Automation in Construction*, **68**: 21 (2016).
2. A. Su and S. J. Al'Aref, *3D Printing Applications in Cardiovascular Medicine* (Eds. J. K. Min, B. Mosadegh, S. Dunham, and S. J. Al'Aref) (Boston: Academic Press: 2018), ch. 1, p. 1.
3. T. D. Ngo, A. Kashani, G. Imbalzano, K. T. Q. Nguyen, and D. Hui, *Composites B: Eng.*, **143**: 172 (2018).
4. I. J. Petrick and T. Simpson, *Research-Technology Management*, **56**, Iss. 6: 12 (2013).
5. M. Attaran, *Business Horizons*, **60**, Iss. 5: 677 (2017).
6. J. Gardan, *Int. J. Production Research*, **54**, Iss. 10: 3118 (2016).
7. B. Rochlitz and D. Pammer, *Periodica Polytechnica Mech. Eng.*, **61**, No. 4: 282 (2017).
8. A. A. Taylor, E. L. Freeman, and M. J. C. van der Ploeg, *Ecotoxicology and Environmental Safety*, **207**: 111458 (2021).
9. K. V. Wong and A. Hernandez, *ISRN Mech. Eng.*, **2012**: 208760 (2012).
10. G. Kynya and P. Ficzere, *Periodica Polytechnica Mech. Eng.*, **67**, No. 2: 143 (2023).
11. D. Ali, A. F. Huayier, and A. Enzi, *Advances in Science and Technology*, **17**, Iss. 4: 130 (2023).
12. M. S. Meiabadi, M. Moradi, M. Karamimoghadam, S. Ardabili, M. Bodaghi, M. Shokri, and A. H. Mosavi, *Polymers*, **13**, Iss. 19: 3219 (2021).
13. T. Yao, Z. Deng, K. Zhang, and S. Li, *Composites B: Eng.*, **163**: 393 (2019).
14. M. M. Hanon, J. Dobos, and L. Zsidai, *Procedia Manufacturing*, **54**: 244 (2021).
15. *D638-14. Standard Test Method for Tensile Properties of Plastics* (ASTM international: 2014).
16. M. Hassan, A. K. Mohanty, and M. Misra, *Mater. Design*, **237**: 112558 (2023).
17. X. Pang, X. Zhuang, Z. Tang, and X. Chen, *Biotechnol. J.*, **5**, Iss. 11: 1125 (2010).
18. I. C. Noyan and J. B. Cohen, *Residual Stress: Measurement by Diffraction and Interpretation* (Springer: 2013).
19. G. R. Yang and X.-J. Wang, *Neuron*, **107**, Iss. 6: 1048 (2020).
20. I. Goodfellow, Y. Bengio, and A. Courville, *Deep Learning* (MIT Press: 2016).
21. T. Hastie, R. Tibshirani, and J. Friedman, T*he Elements of Statistical Learning: Data Mining, Inference, and Prediction* (Springer: 2009), vol. **2**.
22. A. Freddi and M. Salmon, *Design Principles and Methodologies. From Conceptualization to First Prototyping with Examples and Case Studies* (Springer: 2019).
23. S. Salam, T. Choudhary, A. Pugazhendhi, T. N. Verma, and A. Sharma, *Fuel*, **279**: 118469 (2020).
24. R. Chaudhari, J. J. Vora, A. Pramanik, and D. M. Parikh, *Spark Erosion Machining* (Eds. N. K. Jain and K. Gupta) (Boca Raton: CRC Press: 2020), p. 190.
25. M. Mia, P. R. Dey, M. S. Hossain, Md. T. Arafat, Md. Asaduzzaman,

Md. S. Ullah, and S. M. T. Zobaer, *Measurement*, **122**: 380 (2018).
26. R. Benyettou, S. Amroune, S. Mohamed, Y. Seki, and A. Dufresne, *J. Natural Fibers*, **19**, Iss. 17: 15902 (2022).
27. A. Ansari, I. S. Ahmad, A. A. Bakar, and M. R. Yaakub, *IEEE Access*, **8**: 176640 (2020).
28. R. Benyettou, S. Amroune, M. Slamani, and A. Kilic, *Academic J. Manufacturing Eng.*, **21**: 97 (2023).
29. M. Zamouche, H. Tahraoui, Z. Laggoun, S. Mechati, R. Chemchmi, M. I. Kanjal, A. Amrane, A. Hadadi, and L. Mouni, *Processes*, **11**, Iss. 2: 364 (2023).
30. A. R. Kafshgar, S. Rostami, M. R. M. Aliha, and F. Berto, *Procedia Structural Integrity*, **34**: 71 (2021).
31. A. W. Nugroho and C. Budiantoro, *J. Energy Mech. Mater. Manufacturing Eng.*, **4**, No. 1: 29 (2019).
32. H. H. Abdulridha and T. F. Abbas, *Adv. Sci. Technol. Research J.*, **17**, Iss. 6: 49 (2023).
33. R. Teharia, R. M. Singari, and H. Kumar, *Mater. Today: Proc.*, **56**, Pt. 6: 3426 (2022).